IEEE Access
Multidisciplinary ⋮ Rapid Review ⋮ Open Access Journal

Received January 15, 2021, accepted January 26, 2021, date of publication February 2, 2021, date of current version February 9, 2021.

Digital Object Identifier 10.1109/ACCESS.2021.3056458

Effects of Orbital Perturbations on Deployment Dynamics of Tethered Satellite System Using Variable-Length Element

ZHENGFENG BAI[1] AND XIN JIANG[2]
[1]Department of Mechanical Engineering, Harbin Institute of Technology, Weihai 264209, China
[2]Department of Astronautic Engineering, Harbin Institute of Technology, Harbin 150001, China

Corresponding author: Zhengfeng Bai (baizhengfeng@126.com)

ABSTRACT Orbital perturbations caused by the space environment will induce deviations compared with the prescribed motion trajectory or dynamic performance of the tethered satellite system (TSS). To comprehensively investigate the effects of the orbital perturbations on the TSS, a precise variable-length element that can describe the large deformation and flexibility of the tether is adopted in this paper to predict the deployment dynamics considering orbital perturbations, including atmospheric drag, solar pressure, lunisolar gravitation, and J_2 perturbation. To this end, the variable-length element using arbitrary Lagrangian-Eulerian (ALE) description in the frame work of absolute nodal coordinate formulation (ANCF) is developed firstly. Subsequently, the dynamic governing equations for the TSS are established in the context of ANCF with the employment of ANCF reference node (ANCF-RN). Effects of orbital perturbations including atmospheric drag, solar pressure, lunisolar gravity and J_2 perturbation on the dynamics of an optimal deployment are analyzed numerically. It is shown that the orbital perturbations except the J_2 perturbation will induce the out-of-plane motion of the TSS. Additionally, the tether tension is less affected by the orbital perturbations. By contrast, the lunisolar gravitation will induce a deviation on the motion path of satellite, which should be considered in the design phase of the TSS.

INDEX TERMS Tethered satellite system, orbital perturbations, ANCF-ALE, Gauss pseudo-spectral method.

I. INTRODUCTION

Recent decades, increasing attentions have been paid to the tethered satellite system (TSS) with respect to tether dynamics [1], satellite attitude stabilization [2], control strategy [3]. With two or more satellites connected together with the tether, the TSS has wide applications in artificial gravity [4], deep space observation [5], orbital transferring [6], space debris retrieval [7], and so on. Commonly, the satellites of in the TSS system are deployed by a tether [8], which is under the control of a deployment mechanism. For the reason that the tether is thin and is weak to resistance in bending and torsional deformation [9], complex dynamic behaviors could be appeared in the phase of deployment when external perturbation was considered [10]. Being a crucial component for the TSS, dynamics modelling of the tether is fundamental to accurately predict the deployment dynamics of the TSS. Over the past decades, several modes of tether have been proposed, such as the rigid rod model [11], lumped mass model [12], spring mass model [13], and finite element [14], to provide access to dynamic analysis and controller design. For instance, the dumbbell model was adopted to research the deployment dynamics in a low-eccentricity orbit using adaptive sliding mode controller [15]. Ma and Sun [16] proposed an adaptive sliding mode control law based on the rigid model that can deploy the satellite with smaller overshoot of the in-plane angle.

Space environment would induce an undesired influence on the dynamics of TSS deployment [17]. Numerous investigations have been performed by employing the aforementioned modes of the tether. Using the rigid rod model, effect of the atmospheric drag perturbation on a tether-assisted deorbit system was investigated [18], which indicated that the atmospheric drag perturbation would induce offset of the deployment track to a certain extent. A linear stability analysis on a triple-mass TSS in was also exhibited

The associate editor coordinating the review of this manuscript and approving it for publication was Hassen Ouakad.

by Razzaghi and Assadian [19]. Based on the rod model, Wu *et al.* [20] developed a linearized relative motion model of the TSS considering the J_2 perturbation, and the dynamics of a fuel-optimal deployment was discussed. On the basis of the lumped mass model, Yu and Jin [21] investigated the effect of J_2 perturbation and thermal effect, which indicated that the effect of J_2 perturbation depends on the magnitude of sliding friction. Further, considering the space environment including the J_2 perturbation, the atmospheric drag, and solar pressure, an analytical control low of the tether was presented [22]. Attitude stabilization of the satellite during flexible tether deployment that taking account of the J_2 perturbation forces was investigated [2].

However, difficulties are encountered in precise description of large deformation of tether with the adoption of preceding models. In the premise of available computation capacity, precise mechanics model of the tether is indispensable for the performance evaluation of the TSS. Recently, the absolute node coordinate formulation(ANCF) [23] was shown advantageous in describing large deformation, which has been utilized in a wide range of applications related to large scale motion containing flexible components [24]. In terms of simulation on variable-length body, two methodologies were developed. One is the variable-domain finite element model (VFE) [25], and the other is the arbitrary Lagrangian-Eulerian description in the context of the ANCF (ANCF-ALE) [26]. Also, a thin variable length plate element of ANCF-ALE description was developed in [27] that was applied to a topology optimization of the flexible multibody systems. Luo *et al.* [28] investigated the dynamics of a tethered satellite formation under combination of a linear piecewise deployment and an applied jet force. In this paper, a variable-length element that combines arbitrary Lagrangian and Eulerian description in the framework of ANCF is adopted to take the length variation and large deformation of the tether into account. For the ANCF-ALE variable-length element, additional material coordinates are introduced to represent the mass flow at the boundary of the tether. Furthermore, when the mass flow at the boundary node is vanished, the ANCF-ALE variable-length element degenerates to a conventional ANCF element.

However, few studies have been devoted to researching the effects of orbital perturbations on deployment dynamics using the ANCF-ALE variable-length element, which will be addressed in this paper in the condition of an optimal deployed trajectory. A variable-length element to describe length variation of the tether is developed firstly, and an optimal trajectory of the tether velocity is programmed to take practical constraints into account. After that orbital perturbations including the lunisolar gravitation, to which less attention has been paid in literatures, will also be considered in this paper to investigate the effects on the dynamics of the optimal deployment of the TSS.

This paper is organized as follows. Section 2 derives the dynamic governing equations of the TSS using the variable-length tether element and formulas of the orbital perturbations are presented. In section 3, effects of the orbit perturbations on the dynamics of an optimal deployment is discussed. Finally, we conclude the presented work in section 4.

II. DYNAMIC EQUATIONS OF TTS

The TSS in a Kepler circular orbit is schematically illustrated in Fig.1, which comprises of a master satellite denoted as S1 and a sub-satellite denoted as S2. To describe the motion of the TSS system, the global coordinate frame O_1XYZ and the orbital coordinate frame O_2xyz are introduced, respectively. As to the geocentric inertial coordinate frame O_1XYZ, the O_1X axis is directed toward the ascending node, and the O_1Z coincides with the rotating axis of the earth. The axis O_2x of O_2xyz points to the flight direction and the O_2z directs toward the earth's center. The axes O_1Y and O_2y can be acquired by the right-hand rule. Therefore, the position of the TSS can be determined by the in-plane angle θ and the out-of-plane angle φ.

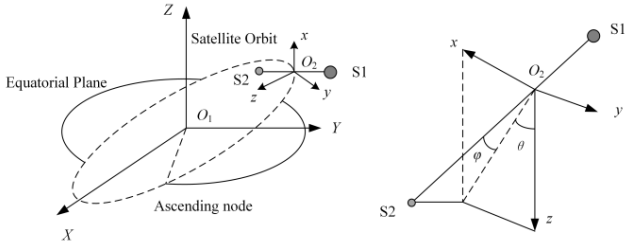

FIGURE 1. Schematic of the TSS.

A. DYNAMIC EQUATIONS OF VARIABLE-LENGTH TETHER

Differing from the conventional ANCF elements that adopt vectors of the positions and the slopes as the node coordinates, additional material coordinates are introduced as the generalized coordinates in the ANCF-ALE elements [27], [28]. As shown in Fig.2, the generalized coordinates of a variable-length element are defined as

$$\mathbf{q} = [\mathbf{q}_e^{\mathrm{T}} \quad \mathbf{q}_l^{\mathrm{T}}]^{\mathrm{T}} \tag{1}$$

where $\mathbf{q}_e = \begin{bmatrix}\mathbf{r}_1^{\mathrm{T}} & \mathbf{r}_{1,x}^{\mathrm{T}} & \mathbf{r}_2^{\mathrm{T}} & \mathbf{r}_{2,x}^{\mathrm{T}}\end{bmatrix}^{\mathrm{T}}$ is the vector of ANCF element coordinates, in which $\mathbf{r}_i (i = 1, 2)$ denote the vector of global position vector of the nodes and $\mathbf{r}_{i,x} = \partial\mathbf{r}/\partial\mathbf{x}$ represents the vector of position gradient coordinates obtained by differentiation with respect to the local coordinate x. $\mathbf{q}_l = [l_1 \quad l_2]^{\mathrm{T}}$ is the vector of local material coordinates to represent length variation of the tether. Due to this description, the mass stream going in or out at the node can be described by the derivative of $\mathbf{q}_l$ with respect to time $\dot{\mathbf{q}}_l = \begin{bmatrix}\dot{l}_1 & \dot{l}_2\end{bmatrix}^{\mathrm{T}}$, detailly, if $\dot{l}_i > 0 (i = 1, 2)$ the length of the element will be extended.

Thus, the global position vector of an arbitrary particle in the tether element can be expressed as

$$\mathbf{r} = \mathbf{N}_e \mathbf{q}_e \tag{2}$$

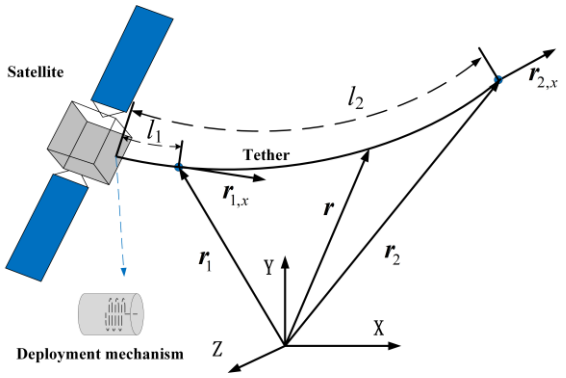

FIGURE 2. Variable-length element.

where $\mathbf{N}_e$ is the shape function matrix, which can be formulated as

$$\mathbf{N}_e = [N_1\mathbf{I}_{3\times3} \quad N_2\mathbf{I}_{3\times3} \quad N_3\mathbf{I}_{3\times3} \quad N_4\mathbf{I}_{3\times3}] \tag{3}$$

in which the entries $N_i(i=1,2,3,4)$ are given below

$$\begin{cases} N_1 = (\xi-1)^2(\xi+2)/4 \\ N_2 = l(\xi-1)^2(\xi+1)/8 \\ N_3 = (\xi+1)^2(-\xi+2)/4 \\ N_4 = l/8(\xi+1)^2(\xi-1) \end{cases} \tag{4}$$

where $\xi = \frac{2l-l_1-l_2}{l_2-l_1}$ $l_1 \le l \le l_2$ and $l = l_2 - l_1$.

According to the Eq.(2), velocity vector and acceleration vector of the arbitrary particle on the element can be acquired by derivation with respect to time, respectively

$$\begin{aligned} \dot{\mathbf{r}} &= \dot{\mathbf{N}}_e\mathbf{q}_e + \mathbf{N}_e\dot{\mathbf{q}}_e \\ \ddot{\mathbf{r}} &= \ddot{\mathbf{N}}_e\mathbf{q}_e + 2\dot{\mathbf{N}}_e\dot{\mathbf{q}}_e + \mathbf{N}_e\ddot{\mathbf{q}}_e \end{aligned} \tag{5}$$

in which we have the following formulations

$$\begin{aligned} \dot{\mathbf{N}}_e &= \frac{\partial\mathbf{N}_e}{\partial l_1}\dot{l}_1 + \frac{\partial\mathbf{N}_e}{\partial l_2}\dot{l}_2 \\ \ddot{\mathbf{N}}_e &= \frac{\partial\mathbf{N}_e}{\partial l_1}\ddot{l}_1 + \frac{\partial^2\mathbf{N}_e}{\partial^2 l_1}\dot{l}_1^2 + 2\frac{\partial^2\mathbf{N}_e}{\partial l_1\partial l_2}\dot{l}_1\dot{l}_2 + \frac{\partial^2\mathbf{N}_e}{\partial^2 l_2}\dot{l}_2^2 + \frac{\partial\mathbf{N}_e}{\partial l_2}\ddot{l}_2 \end{aligned} \tag{6}$$

Thus, Eq. (5) can be transformed into a compact form and is expressed as

$$\begin{aligned} \dot{\mathbf{r}} &= \mathbf{N}\dot{\mathbf{q}} \\ \ddot{\mathbf{r}} &= \mathbf{N}\ddot{\mathbf{q}} + \ddot{\mathbf{r}}_l \end{aligned} \tag{7}$$

where $\mathbf{N} = \begin{bmatrix}\mathbf{N}_e & \mathbf{N}_{e,l_1}\mathbf{q}_e & \mathbf{N}_{e,l_2}\mathbf{q}_e\end{bmatrix}$ denote the extended shape function matrix. $\mathbf{N}_{e,l_i}(i=1,2)$ denote $\partial\mathbf{N}_e/\partial l_i$. $\ddot{\mathbf{r}}_l$ is the additional inertial item that can be clarified as

$$\begin{aligned} \ddot{\mathbf{r}}_l = {} & 2\left(\mathbf{N}_{e,l_1}\dot{l}_1 + \mathbf{N}_{e,l_2}\dot{l}_2\right)\dot{\mathbf{q}}_e \\ & + \left(\mathbf{N}_{e,l_1l_1}\dot{l}_1^2 + 2\mathbf{N}_{e,l_1l_2}\dot{l}_1\dot{l}_2 + \mathbf{N}_{e,l_2l_2}\dot{l}_2^2\right)\mathbf{q}_e \end{aligned} \tag{8}$$

where $\mathbf{N}_{e,l_il_j}(i,j=1,2)$ denote $\frac{\partial\mathbf{N}_e}{\partial l_i\partial l_j}$.

Herein the D'Alembert's principle is used to derive the motion governing equations due to its application in time-varying system. For the variable-length tether element of length l, the total virtual work done by all external forces and inertial forces in an arbitrary virtual displacement should be vanished

$$\int_{l_1}^{l_2} \delta\mathbf{r}^{\mathrm{T}}\left(\mathbf{F}_f + \mathbf{F}_e + \mathbf{F}_d - \rho A\ddot{\mathbf{r}}\right) dl = 0 \tag{9}$$

where $\mathbf{F}_f$ denote the external perturbation forces and $\mathbf{F}_e$ is the elastic force, $\mathbf{F}_d$ the damping force that constrained by the linear viscoelasticity law [29]. ρ and A are the density and cross-sectional area of the tether element, respectively.

Items in Eq.(9) can be formulated elaborately as

$$\begin{aligned} & \int_{l_1}^{l_2} \delta\mathbf{r}^{\mathrm{T}}\mathbf{F}_f dl \\ & = \delta\mathbf{q}^{\mathrm{T}}\frac{l_e}{2}\int_{-1}^{1}\mathbf{N}^{\mathrm{T}}\mathbf{F}_f d\xi \\ & \int_{l_1}^{l_2} \delta\mathbf{r}^{\mathrm{T}}\left(\mathbf{F}_e + \mathbf{F}_d\right) dl \\ & = -\delta\mathbf{q}^{\mathrm{T}}\frac{l_e}{2}\int_{-1}^{1}\left[\left(\frac{\partial\varepsilon}{\partial\mathbf{q}}\right)^{\mathrm{T}} EA(\varepsilon+c\dot{\varepsilon}) + \left(\frac{\partial\kappa}{\partial\mathbf{q}}\right)^{\mathrm{T}} EI(\kappa+c\dot{\kappa})\right] \\ & \quad \times d\xi \int_{l_1}^{l_2} \delta\mathbf{r}^{\mathrm{T}}(-\rho A\,\ddot{\mathbf{r}})dl = -\delta\mathbf{q}^{\mathrm{T}}\frac{l_e}{2}\int_{-1}^{1}\rho A\mathbf{N}^{\mathrm{T}}\ddot{\mathbf{r}}\,d\xi \end{aligned} \tag{10}$$

where c is the coefficient of damping, E and I are the modulus of elasticity and second moment of the cross-sectional area, respectively. The axial strain ε and the curvature of the element can be calculated with the following expression, respectively

$$\begin{aligned} \varepsilon &= \frac{1}{2}\left(\mathbf{r}_{,l}^{\mathrm{T}}\mathbf{r}_{,l} - 1\right) \\ \kappa &= \frac{\left\|\mathbf{r}_{,l}\times\mathbf{r}_{,ll}\right\|}{\left\|\mathbf{r}_{,l}\right\|^3} \end{aligned} \tag{11}$$

Due to the arbitrary property of $\delta\mathbf{r}^{\mathrm{T}}$ in Eq.(9), the dynamic equations of the element can be derived

$$\mathbf{M}_e\ddot{\mathbf{q}} + \mathbf{Q}_i + \mathbf{Q}_e + \mathbf{Q}_f = \mathbf{0} \tag{12}$$

in which

$$\begin{aligned} \mathbf{M}_e &= \frac{l_e}{2}\int_{-1}^{1}\rho A\mathbf{N}^{\mathrm{T}}\mathbf{N}d\xi \\ \mathbf{Q}_i &= \frac{l_e}{2}\int_{-1}^{1}\rho A\mathbf{N}^{\mathrm{T}}\ddot{\mathbf{r}}_l d\xi \\ \mathbf{Q}_e &= \frac{l_e}{2}\int_{-1}^{1}\left[\left(\frac{\partial\varepsilon}{\partial\mathbf{q}}\right)^{\mathrm{T}} EA(\varepsilon+c\dot{\varepsilon}) + \left(\frac{\partial\kappa}{\partial\mathbf{q}}\right)^{\mathrm{T}} EI(\kappa+c\dot{\kappa})\right]d\xi \\ \mathbf{Q}_f &= -\frac{l_e}{2}\int_{-1}^{1}\mathbf{N}^{\mathrm{T}}\mathbf{F}_f d\xi \end{aligned} \tag{13}$$

where $\mathbf{M}_e$ is the time-dependent mass matrix of the element, $\mathbf{Q}_i$ is the additional inertial force resulted from time-varying of material coordinates. $\mathbf{Q}_e$ denotes the generalized fore associated with elastic deformation and damping, and $\mathbf{Q}_f$ is the generalized external forces.

Considering a long variable-length tether discretized with N nodes, which is assembled with two length time-varying element attached on the tether boundary, and N-3 internal elements with constant length. Thus, the dynamic governing equations of a tether can be obtained by assembling all the tether elements with inter-connectivity conditions

$$\mathbf{M}_t\ddot{\mathbf{q}}_t + \mathbf{Q}_t = \mathbf{0} \tag{14}$$

where $\mathbf{q}_t = \begin{bmatrix}\mathbf{r}_1^{\mathrm{T}} & \mathbf{r}_{1,l}^{\mathrm{T}} & \mathbf{r}_2^{\mathrm{T}} & \mathbf{r}_{2,l}^{\mathrm{T}} & \dots & \mathbf{r}_N^{\mathrm{T}} & \mathbf{r}_{N,l}^{\mathrm{T}} & l_1 & l_2\end{bmatrix}$ is the vector of generalized coordinates of the tether, $\mathbf{M}_t$ and $\mathbf{Q}_t$ are the corresponding mass matrix and generalized force vector of the tether. It is noted that excessively long or short lengths of the tether variable-length element would reduce the accuracy of the numerical result. Therefore, an operation of inserting or removing nodes is introduced to the boundary element. When the length of the element is longer than the given maxim length, new nodes are inserted into the boundary element. Similarly, when the length of the element is shorter than the given minimum length, the nodes inside the element are removed. More description of the procedure for nodes inserting or removal can refer to [26].

B. FORMULATIONS OF ORBITAL PERTURBATIONS

The J_2 perturbation is resulted from the irregular shape of the earth [30], the gravitational acceleration in this case can be written as

$$\mathbf{g} = -\frac{\mu_E}{|\mathbf{r}_s|^2}\left[1 - \frac{R_E^2}{|\mathbf{r}_s|^2}J_2\mathrm{P}_2(\sin\phi)\right]\frac{\mathbf{r}_s}{|\mathbf{r}_s|} \tag{15}$$

where $\mu_E = 3.986 \times 10^{14} m^3/s^2$ is the gravitational constant of the Earth. $R_E = 6378\ km$ denotes Earth's equatorial radius and $J_2 = 1.0826 \times 10^{-3}$ is the harmonic coefficient. P_2 means the Legendre polynomials with order 2, and ϕ is the geocentric latitude. $\mathbf{r}_s$ denotes the position vector of the satellites with respect to Geocentric inertial frame.

It is mentioned that under the condition of ignoring J_2 item, Eq. (15) will degenerate into the regular spherical gravitational perturbation of the earth, which is the case of no perturbation considered in this paper.

Formulation of the atmospheric drag force can be expressed straightly as follows

$$\mathbf{F}_d = -\frac{1}{2}\rho C_D S\mathbf{v}_r|\mathbf{v}_r| \tag{16}$$

where C_D is the drag coefficient and S the frontal area of the satellites. $\mathbf{v}_r$ is the relative velocity of satellites to the atmosphere, which can be obtained by the following expression under the assumption that the atmosphere rotates with the earth

$$\mathbf{v}_r = \mathbf{v}_s - \boldsymbol{\omega}_\mathbf{E} \times \mathbf{r}_s \tag{17}$$

where $\mathbf{v}_s$ and $\mathbf{r}_s$ are the inertial velocity vector and position vector of the satellites, respectively. $\boldsymbol{\omega}_E$ is the angular velocity of the earth.

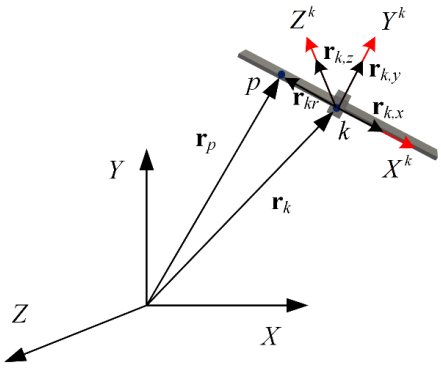

FIGURE 3. ANCF-RN description.

The perturbing force on the satellites due to the radiation pressure can be formulated as

$$\mathbf{F} = -\vartheta P_{SR} C_R A_{sc}\hat{\mathbf{u}} \tag{18}$$

where $P_{SR} = 4.56\mu\mathrm{Pa}$ denotes the solar radiation pressure. A_{sc} is the absorbing area of the satellites. ϑ is the shadow function with value 0 or 1, in which $\vartheta = 1$ represents the satellites in the earth's shadow, otherwise $\vartheta = 0$. C_R is the radiation pressure that varies from 1 and 2. $\hat{\mathbf{u}}$ is the unit vector pointing toward the sun from the satellite.

The perpetuating acceleration induced by the lunisolar gravitation is expressed as

$$\mathbf{p}_* = \mu_*\left(\frac{\mathbf{r}_{*/s}^3}{r_{*/s}^3} - \frac{\mathbf{r}_*}{r_*^3}\right) \tag{19}$$

where the symbol $* = m, o$ denotes the moon or the sun, respectively. μ_* denote the gravitational parameter for the moon $\mu_m = 4903 km^3/s^2$ and $\mu_s = 132.712(10^9) km^3/s^2$ for the sun. $\mathbf{r}_*$ is the position vector of the moon or sun relative to the earth and the $\mathbf{r}_{*/s}$ means the position of the moon or sun relative to the satellite. Detailed information for the inertial position vector $\mathbf{r}_*$ can be referred to [31].

C. DYNAMIC EQUATIONS OF TSS

Dynamic equations of the TSS can be obtained with the employment of the ANCF-RN [32], in which the rigid body was described in the frame work of ANCF mesh. As shown in Fig.3, the coordinates of a three-dimensional ANCF-RN are defined as

$$\mathbf{q}_k = \begin{bmatrix}\mathbf{r}_k^{\mathrm{T}} & \mathbf{r}_{k,x}^{\mathrm{T}} & \mathbf{r}_{k,y}^{\mathrm{T}} & \mathbf{r}_{k,z}^{\mathrm{T}}\end{bmatrix} \tag{20}$$

where $\mathbf{r_k}$ is the position vector of node k, $\mathbf{r}_{k,x}, \mathbf{r}_{k,y}, \mathbf{r}_{k,z}$ are vectors parallel to the axes of ANCF-RN local coordinate system, respectively. Additionally, following six constraints are added to describe the rigid motion of the satellites

$$\begin{cases}\|\mathbf{r}_{k,x}\| = 1, \|\mathbf{r}_{k,y}\| = 1, \|\mathbf{r}_{k,z}\| = 1 \\ \mathbf{r}_{k,x}\cdot\mathbf{r}_{k,y} = \mathbf{0}, \mathbf{r}_{k,x}\cdot\mathbf{r}_{k,y} = \mathbf{0}, \mathbf{r}_{k,y}\cdot\mathbf{r}_{k,z} = \mathbf{0}\end{cases} \tag{21}$$

Thus, the position vector of an arbitrary point on the satellite can be derived as

$$\mathbf{r}_p = \mathbf{r}_k + \mathbf{r}_{kr} \tag{22}$$

where $\mathbf{r}_{kr}$ is the local position vector and can be formulated as

$$\mathbf{r}_{kr} = [\mathbf{r}_{k,x}\mathbf{r}_{k,y}\mathbf{r}_{k,z}][xyz]^{\mathrm{T}} \tag{23}$$

where (x, y, z) is the coordinates of the local position of the arbitrary point on the rigid body.

Substitute Eq.(23) into Eq.(22), Eq.(22) can be recast as

$$\begin{aligned}\mathbf{r}_p &= \mathbf{r}_k + [\mathbf{r}_{k,x}\mathbf{r}_{k,y}r_{k,z}][xyz]^{\mathrm{T}} \\ &= \mathbf{S}_r\mathbf{q}_k\end{aligned} \tag{24}$$

where $\mathbf{S}_r$ is the shape function of the reference node.

The constant symmetrical mass matrix of the ANCF reference node can be obtained by

$$\mathbf{M}_r = \int_{V_r} \rho_r \mathbf{S}_r^{\mathrm{T}}\mathbf{S}_r dV \tag{25}$$

where ρ_r and V_r are the material density and spatial domain of the rigid body.

In order to connect the satellites to the tether, the following linear constraint equations is imposed

$$\mathbf{r}_k = \mathbf{r} \tag{26}$$

where $\mathbf{r}$ is the global position of the node on the tether, $\mathbf{r}_k$ is the global position of the reference node.

The nonlinear constraint equations Eq.(21) and the linear constraint equation Eq.(26) can be written in a vector form as $\mathbf{\Phi}(\mathbf{q}, \mathbf{t}) = \mathbf{0}$.Using the Lagrangian multiplier method, dynamic equations of the TSS can be derived in a compact form and expressed as

$$\begin{aligned}\mathbf{M}\ddot{\mathbf{q}} + \mathbf{\Phi}_{\mathbf{q}}^{\mathrm{T}}\lambda + \mathbf{F}(\mathbf{q}) &= \mathbf{Q}(\mathbf{q}) \\ \mathbf{\Phi}(\mathbf{q}, \mathbf{t}) &= \mathbf{0}\end{aligned} \tag{27}$$

where $\mathbf{q} = \left[\mathbf{q}_\mathbf{t}^{\mathrm{T}}\mathbf{q}_\mathbf{k}^{\mathrm{T}}\right]^{\mathrm{T}}$ is the generalized coordinates of system, $\mathbf{M}$ is the system mass matrix, and $\mathbf{\Phi}(\mathbf{q}, \mathbf{t})$ is the vector of constraint equations. $\mathbf{\Phi}_\mathbf{q}$ is the Jacobian matrix of constraint equations. $\mathbf{F}(\mathbf{q})$ and $\mathbf{Q}(\mathbf{q})$ are the system generalized elastic forces and generalized external perturbation forces respectively. Numerical integration of generalized-alpha method [33] is adopted to pursue the numerical solution of Eq.(27).After substitution of the foregoing equations Eqs.(15-19) that formulate the orbital perturbations into the Eq.(27) in a generalized form, dynamic equations of the TSS considering orbital perturbations are obtained. It is noted that due to the variation of the tether length, the mass matrix of the system is time-dependent. Therefore, mass matrix of the system must be Cholesky factorized at each integration, which can degenerate the computational efficiency.

III. DYNAMIC ANALYSIS OF TSS

A. OPTIMAL TRAJECTORY PROGRAMMING

To take practical constraint states into account, an optimal procedure for the tether deployment using nonlinear programming is performed in this section. Herein, the Gauss pseudo-spectral method [34], which transforms the continuous optimal control problem into nonlinear programming, is employed to project the optimal trajectory of tether velocity that satisfies the dynamic constraints. It's noted that the optimal trajectory is obtained with the dumbbell model, which was usually adopted in the optimal control of TSS [35].

The time interval in the Gauss pseudo-spectral method is transformed from $[t_0, t_f]$ into $[-1,1]$ with interpolation of discretized points firstly. Then a nonlinear programming procedure is conducted to search the optimal solutions, which satisfies the boundary conditions and the dynamic constraints. In this paper, the vector of the selected state variables in the optimal procedure is defined as

$$\mathbf{x} = \left[L\ \dot{L}\ \theta\ \dot{\theta}\ \varphi\ \dot{\varphi}\right] \tag{28}$$

in which L denotes the length of the tether, and θ, φ are the in-plane angel and out-of-plane angle, respectively. The tether tension T in the dumbbell model is defined as the control variable, which subject to an inequality constraint given in Eq. (29) to avoid the slack phenomenon of the tether.

$$T_{\min} < T < T_{\max} \tag{29}$$

where $T_{\min}$ and $T_{\max}$ are the minimum or maximum amplitude of the tether tension. The constrains used in the optimal procedure is explicitly shown in Table 1.

TABLE 1. Constraints in optimization.

State variables	Boundary constraints		Path constraints
	Initial	Final	
L (m)	2	1000	2~1000
$\dot{L}$ (m / s)	0~1	0	0~1
θ (rad)	0	0	$-\pi/3 \sim \pi/3$
$\dot{\theta}$ (rad / s)	0	$-\pi/40 \sim \pi/40$	$-\pi/15 \sim \pi/15$
T (N)	0~5	0~5	0~5

To guarantee a relatively smooth deployment characterized with slowly variation of both tether length and in-plane angle, the objective function of the optimal procedure is defined as

$$J = \int (\ddot{L} + \ddot{\theta})dt \tag{30}$$

B. EFFECTS OF ORBITAL PERTURBATION

In this section, dynamic simulations in condition of different cases considering single or multi factors of orbital perturbations, as listed in Table 2, are presented. Additionally, parameters used in the numerical simulation are displayed in Table 3.

The optimal trajectory of tether velocity programmed in section 3.1 is depicted in Fig.4, in which a deployed phase

TABLE 2. Description of different cases.

Cases	Perturbations
1	Without perturbation
2	Atmospheric drag perturbation
3	Solar pressure perturbation
4	Lunisolar gravitation perturbation
5	J_2 perturbation
6	All perturbations

TABLE 3. Parameters used in simulation.

Parameter	Value
S1 mass	100 kg
Tether density	1350 kg/m^3
Tether diameter	0.002 m
Orbital radius	6887×10^3 m
Atmospheric density	1.7×10^{-12} kg/m^3
S2 mass	90 kg
Tether modulus	2.6×10^{10} Pa
Poisson rate	0.3
Total tether length	1000 m
Radiation pressure coefficient	1.3
Absorbing area of satellite	0.56 m^2

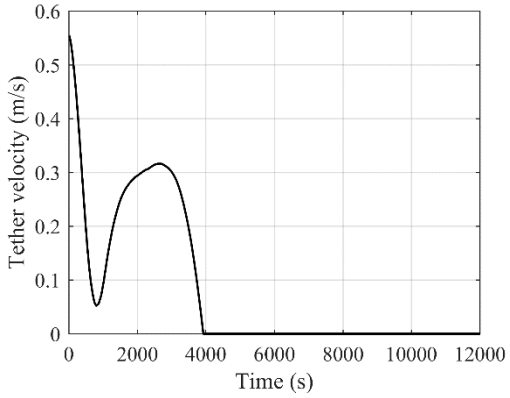

FIGURE 4. Tether velocity.

with variable-length of the tether and a station-keeping phase with constant length of the tether are trajected.

Responses of the in-plane angle under different conditions of orbital perturbations are exhibited in Fig.5. Obviously, a good agreement on the variation of the in-plane angle indicates that a relatively slight effect is induced by the orbital perturbations on the in-plane motion of the TSS. Due to the optimal programming of tether velocity, the in-plane angles swing with magnitude of 45 deg in deployed phase and keep varying periodically with amplitude of 8.4 deg.

Fig.6 exhibits the relative distance between the satellites over the duration of deployment and station-keeping. Obviously, a smooth and reliable deployment can be observed due to the consideration of dynamic constraints in the optimal procedure. Note that the curves from different cases agree well, which indicate the orbital perturbations have no

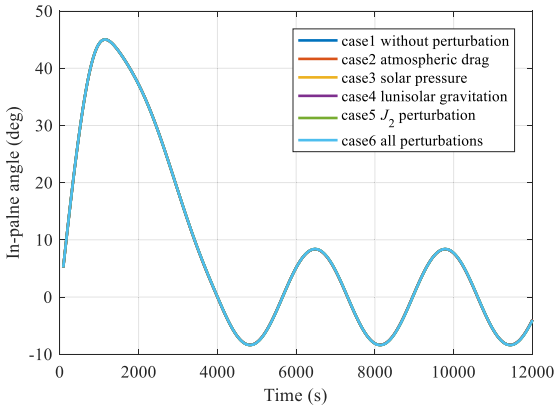

FIGURE 5. In-plane angle.

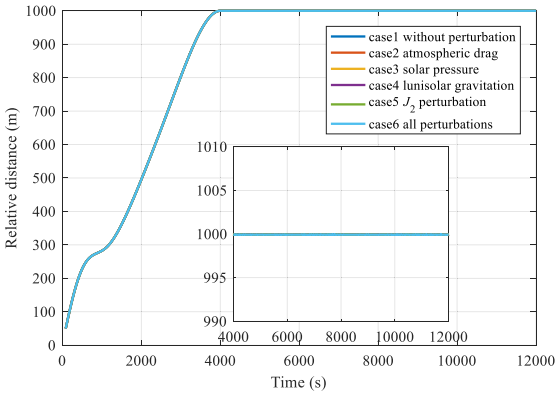

FIGURE 6. Relative distance.

influence on the relative distance during the phases of deployment and station-keeping.

Fig.7 displays the responses of out-of-plane angle for the TSS optimal deployment, in which an obvious deviation can be observed between the different cases. Differing from the unchanged tendency in both case1 and case5, the out-of-plane angle changes variously for the other cases. From Fig.7(a), it can be seen that the atmospheric drag in case 1 will induce a small unpredictable variation during the phase of station-keeping. By contrast, the solar pressure will change the out-of-plane angle with amplitude of 7.2×10^{-5} deg during the deployment phase compared with what in station-keeping phase. Additionally, the fact that the J_2 perturbation cannot induce the motion of out-of-plane can be observed in Fig.7(b) through response variation of case 5. Effect of the lunisolar gravity can be revealed in the case 4, wherein a significant change of out-of-plane angle is appeared in the phase of station-keeping. In conclusion, the solar pressure perturbation plays a primary role in the phase of deployment while the lunisolar gravity plays a primary role in the phase of station-keeping.

The relative in-plane motion trajectory of the TSS is depicted in Fig.8. Similar to the in-plane angle, the orbital perturbations have no influence on the in-plane relative motion of the TSS. During the deployment for each case, the amplitude of the relative motion swings around 310 m and forms into a liberation with amplitude of 150 m in the phase of station-keeping.

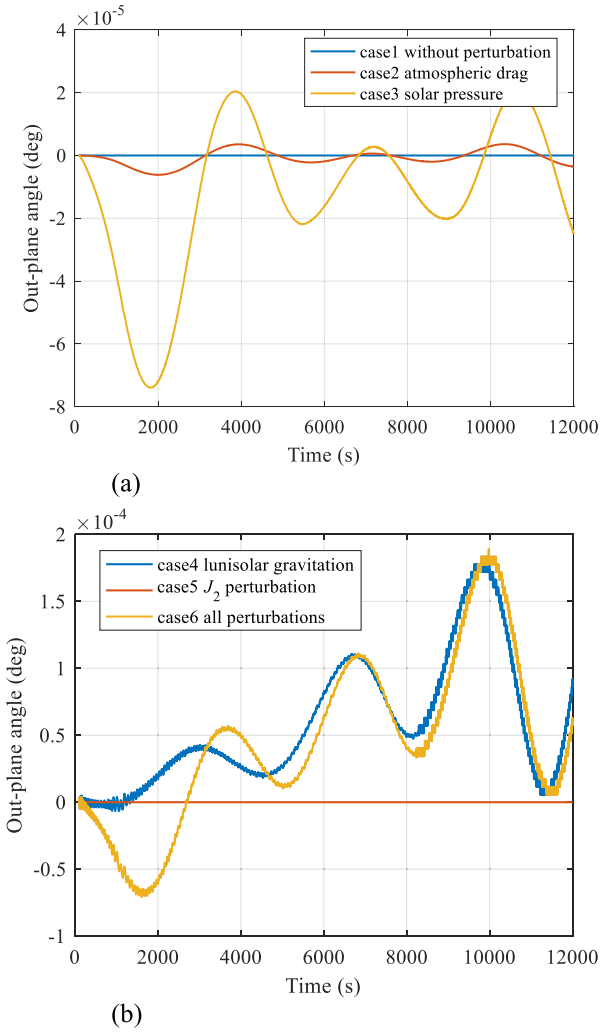

FIGURE 7. Out-of-plane angel.

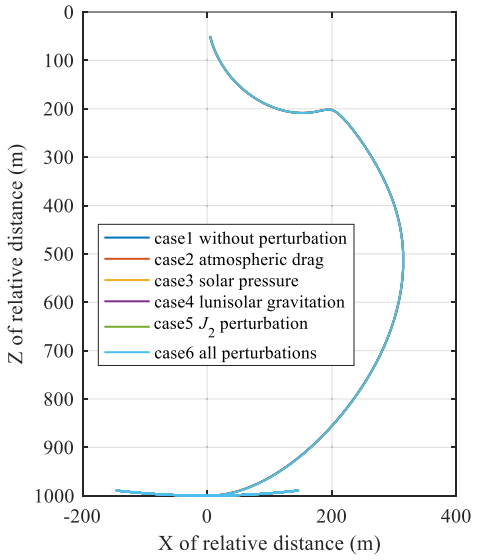

FIGURE 8. In-plane relative motion.

To analysis the effect of orbital perturbations on the out-of-plane motion, Fig.9 exhibits the out-of-plane trajectories of relative motion for all cases, respectively. It can be

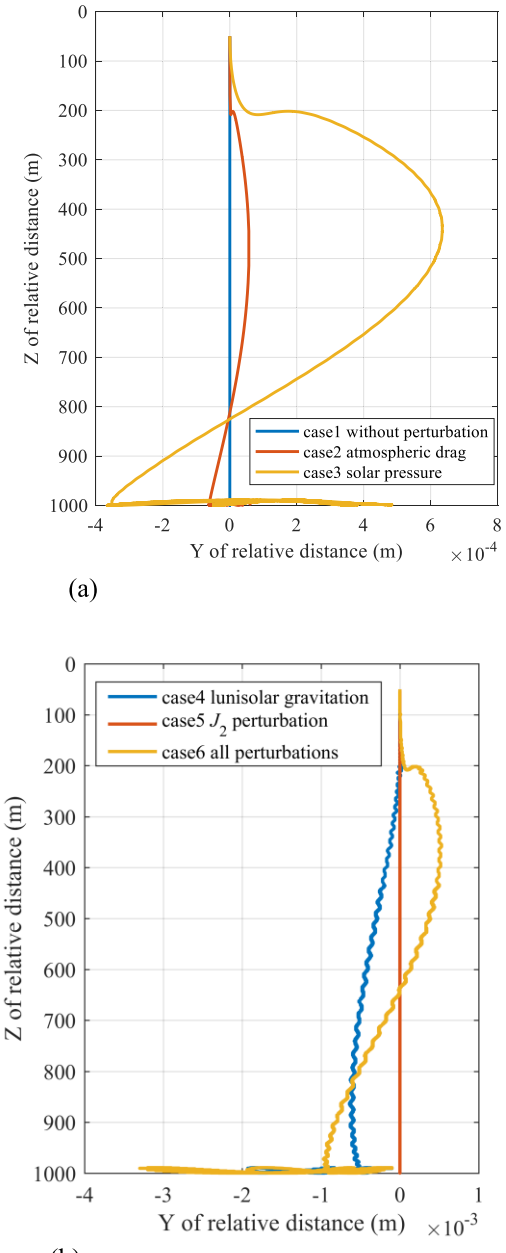

FIGURE 9. Out-of-plane relative motion.

seen from Fig.9(a) that the deviation caused by solar pressure during deployment is relatively more intense compared with other cases. Meanwhile, the lunisolar gravity affects the out-of-plane motion more significantly in the phase of station-keeping.

Responses of the tether tension for different cases are illustrated in Fig. 10 respectively, in which an obvious increase and a periodical oscillation in the amplitude of the tether tension can be observed. It is noted that the tension variation is influenced seldomly by the orbital perturbations. Furthermore, around the instant of time $t = 1000$ s, there is an obvious oscillation on the tension response, and it is noted that the tether velocity experiences a rapid change during that period, which implies that the variation ratio of

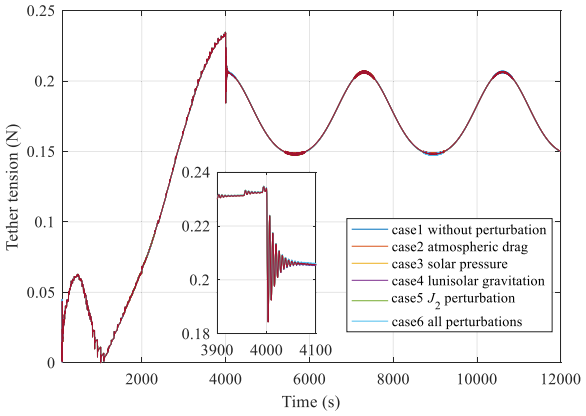

FIGURE 10. Tether tension.

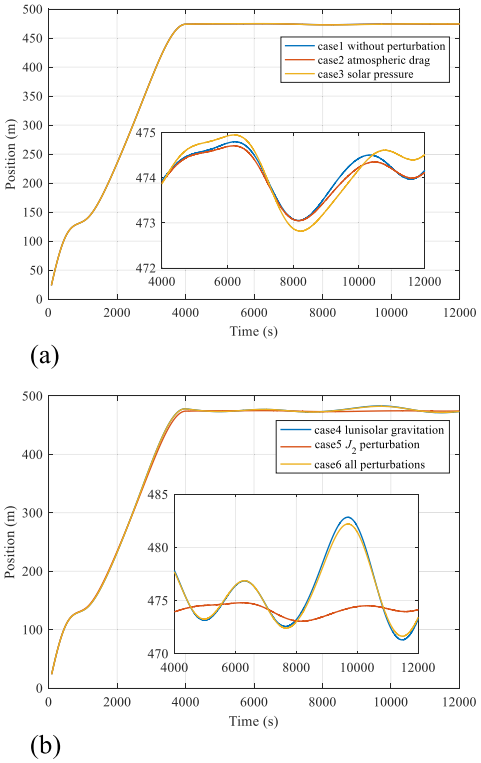

FIGURE 11. Position response of S1.

the tether velocity affects the tension response significantly. This conclusion can also be verified by the phenomenon of rapidly drop and shake of the tether tension at the instant of $t = 4000$ s.

Position response of the master satellite S1 is depicted in Fig.11, in which a smoothly deployment can be observed. From the responses from case1 to case3 in the Fig.11(a), it can be found that the orbital perturbations have less influence on the position response. By contrast, as shown in Fig11(b), an obvious deviation is appeared during the phase of station-keeping in the case 5 and case 6, which implies that the lunisolar gravity will induce the deviation on the motion path of satellites, rather than change the path of relative motion between the master satellite and the sub-satellite.

Additionally, in order to validate the effectiveness of the results obtained in this work, the results obtained in this work are comparing with the results in literature [18], [36], [37]. In the work presented by Pernicka *et al.* [36], the dynamics of a short tethered satellite system considering the effects of perturbations of solar and gravity, atmospheric drag, and solar radiation pressure are discussed. It showed that the perturbations would induce deployment error, which will lead to libration of the tether, but tension will still be maintained. This statement is consistent with the observation in this work. Specially, from a convincible perspective, the observations, that J_2 perturbation will induce some offset of the deployment of the TSS in-plane while has no influence on the out-of-plane motion of the system, can be supported by conclusion presented in Zheng's work [37]. Also, the results obtained by the literature [18] showed that the atmospheric drag will induce unpredictable out-of-plane motion, which is consistent with the results of this work. So, the effectiveness of the results obtained by the numerical simulation results in this work are verified.

IV. CONCLUSION

In this paper, the effect of orbital perturbations including lunisolar gravitation on the deployment dynamics of the TSS is presented to comprehensively investigate the deviations caused by orbital perturbations. To describe the length variation of the tether, a variable-length element of the tether that is characterized with precise description of large deformation is used to derive the governing dynamic equations. Additionally, an optimal trajectory of tether velocity optimized by nonlinear dynamic programming that takes practical state constraints into account is adopted in the deployment phase. Based on the derived differential algebraic equations (DAES) and the optimal release velocity of tether, subsequently effects of orbital perturbations including atmospheric drag, solar pressure, lunisolar gravity and the J_2 perturbation on the dynamic characteristics are discussed.

Numerical results indicate that the J_2 perturbations has less effect on the dynamic behavior during the TSS deployment. On the other hand, the out-of-plane angle would be affected by the perturbations comprise of atmospheric drag, solar pressure and lunisolar gravity. In detail, the atmospheric drag induces an unpredictable change in the out-of-plane angle with a small amplitude. By contrast, in the deployed phase, a large deviation on the out-of-plane angel is caused by the solar pressure, while in the phase of station-keeping, the lunisolar gravity has a significant influence on the out-of-plane motion. Furthermore, all the orbital perturbations presented in this work have slightly effects on the variation of the tether tension both in the phase of deployment and station-keeping. As a point of attention, the lunisolar gravity will induce a deviation on the motion path of satellite, which should be considered in the design phase of the TSS.

REFERENCES

[1] B. S. Yu, H. Wen, and D. P. Jin, "Review of deployment technology for tethered satellite systems," *Acta Mechanica Sinica*, vol. 34, no. 4, pp. 754–768, Aug. 2018, doi: 10.1007/s10409-018-0752-5.

[2] C. Luo, H. Wen, and D. Jin, "Deployment of flexible space tether system with satellite attitude stabilization," *Acta Astronautica*, vol. 160, pp. 240–250, Jul. 2019, doi: 10.1016/j.actaastro.2019.04.036.

[3] G. Sun and Z. H. Zhu, "Fractional order tension control for stable and fast tethered satellite retrieval," *Acta Astronautica*, vol. 104, no. 1, pp. 304–312, Nov. 2014, doi: 10.1016/j.actaastro.2014.08.012.

[4] M. D. Jokic and J. M. Longuski, "Artificial gravity and abort scenarios via tethers for human missions to mars," *J. Spacecraft Rockets*, vol. 42, no. 5, pp. 883–889, Sep. 2005, doi: 10.2514/1.6121.

[5] P. Bainum and Z. Tan, "Tethered satellite constellations in auroral observation missions," in *Proc. AIAA/AAS Astrodynamics Spec. Conf. Exhibit*, Aug. 2002, pp. 1–9, doi: 10.2514/6.2002-4640.

[6] G. Shi, Z. Zhu, and Z. H. Zhu, "Stable orbital transfer of partial space elevator by tether deployment and retrieval," *Acta Astronautica*, vol. 152, pp. 624–629, Nov. 2018, doi: 10.1016/j.actaastro.2018.09.013.

[7] S. B. Khan and J. R. Sanmartin, "Analysis of tape tether survival in LEO against orbital debris," *Adv. Space Res.*, vol. 53, no. 9, pp. 1370–1376, May 2014, doi: 10.1016/j.asr.2014.02.008.

[8] M. Kruijff and E. J. van der Heide, "Qualification and in-flight demonstration of a European tether deployment system on YES2," *Acta Astronautica*, vol. 64, nos. 9–10, pp. 882–905, May 2009, doi: 10.1016/j.actaastro.2008.10.014.

[9] J. Lim and J. Chung, "Dynamic analysis of a tethered satellite system for space debris capture," *Nonlinear Dyn.*, vol. 94, no. 4, pp. 2391–2408, Dec. 2018, doi: 10.1007/s11071-018-4498-1.

[10] M. Kruijff, E. van der Heide, W. Ockels, and E. Gill, "First mission results of the YES2 tethered SpaceMail experiment," in *Proc. AIAA/AAS Astrodynamics Spec. Conf. Exhibit*, Aug. 2008, pp. 1–29, doi: 10.2514/6.2008-7385.

[11] G. Zhao, L. Sun, S. Tan, and H. Huang, "Librational characteristics of a dumbbell modeled tethered satellite under small, continuous, constant thrust," *Proc. Inst. Mech. Eng., G, J. Aerosp. Eng.*, vol. 227, no. 5, pp. 857–872, May 2013, doi: 10.1177/0954410012445845.

[12] S. Yu, "Dynamic model and control of mass-distributed tether satellite system," *J. Spacecraft Rockets*, vol. 39, no. 2, pp. 213–218, Mar. 2002, doi: 10.2514/2.3822.

[13] V. V. Sidorenko and A. Celletti, "A 'spring–mass' model of tethered satellite systems: Properties of planar periodic motions," *Celestial Mech. Dyn. Astron.*, vol. 107, nos. 1–2, pp. 209–231, Jun. 2010, doi: 10.1007/s10569-010-9275-5.

[14] M. J. Leamy, A. K. Noor, and T. M. Wasfy, "Dynamic simulation of a tethered satellite system using finite elements and fuzzy sets," *Comput. Methods Appl. Mech. Eng.*, vol. 190, nos. 37–38, pp. 4847–4870, 2001, doi: 10.1016/S0045-7825(00)00352-2.

[15] C. Wang, P. Wang, A. Li, and Y. Guo, "Deployment of tethered satellites in low-eccentricity orbits using adaptive sliding mode control," *J. Aerosp. Eng.*, vol. 30, no. 6, 2017, Art. no. 04017077, doi: 10.1061/(asce)as.1943-5525.0000793.

[16] Z. Ma and G. Sun, "Adaptive sliding mode control of tethered satellite deployment with input limitation," *Acta Astronautica*, vol. 127, pp. 67–75, Oct. 2016, doi: 10.1016/j.actaastro.2016.05.022.

[17] B. Yu, D. Jin, and H. Wen, "Nonlinear dynamics of flexible tethered satellite system subject to space environment," *Appl. Math. Mech.*, vol. 37, no. 4, pp. 485–500, Apr. 2016, doi: 10.1007/s10483-016-2049-9.

[18] X. Cao, P. Zheng, and S. Zhang, "Atmospheric drag perturbation effect on the deployment of tether-assisted deorbit system," in *Proc. Int. Conf. Mechatronics Autom.*, Aug. 2009, pp. 4316–4321, doi: 10.1109/ICMA.2009.5246565.

[19] P. Razzaghi and N. Assadian, "Study of the triple-mass tethered satellite system under aerodynamic drag and J_2 perturbations," *Adv. Space Res.*, vol. 56, no. 10, pp. 2141–2150, Nov. 2015, doi: 10.1016/j.asr.2015.07.046.

[20] B. Wu, G. Xu, and X. Cao, "Relative dynamics and control for satellite formation: Accommodating J_2 perturbation," *J. Aerosp. Eng.*, vol. 29, no. 4, 2016, Art. no. 04016011, doi: 10.1061/(asce)as.1943-5525.0000600.

[21] B. S. Yu and D. P. Jin, "Deployment and retrieval of tethered satellite system under J_2 perturbation and heating effect," *Acta Astronaut.*, vol. 67, nos. 7–8, pp. 845–853, 2010, doi: 10.1016/j.actaastro.2010.05.013.

[22] B. S. Yu, D. P. Jin, and H. Wen, "Analytical deployment control law for a flexible tethered satellite system," *Aerosp. Sci. Technol.*, vol. 66, pp. 294–303, Jul. 2017, doi: 10.1016/j.ast.2017.02.026.

[23] A. A. Shabana, "Computer implementation of the absolute nodal coordinate formulation for flexible multibody dynamics," *Nonlinear Dyn.*, vol. 16, no. 3, pp. 293–306, 1998, doi: 10.1023/A:1008072517368.

[24] J. Gerstmayr, H. Sugiyama, and A. Mikkola, "An overview on the developments of the absolute nodal coordinate formulation," in *Proc. 2nd Joint Int. Conf. Multibody Syst. Dyn.*, 2012, pp. 1–12.

[25] M. Fujiwara, S. Takehara, and Y. Terumichi, "Numerical approach to modeling flexible body motion with large deformation, displacement and time-varying length," *Mech. Eng. J.*, vol. 4, no. 4, p. 17-30, 2017, doi: 10.1299/mej.17-00030.

[26] J. L. Tang, G. X. Ren, W. D. Zhu, and H. Ren, "Dynamics of variable-length tethers with application to tethered satellite deployment," *Commun. Nonlinear Sci. Numer. Simul.*, vol. 16, no. 8, pp. 3411–3424, Aug. 2011, doi: 10.1016/j.cnsns.2010.11.026.

[27] J. Sun, Q. Tian, H. Hu, and N. L. Pedersen, "Topology optimization of a flexible multibody system with variable-length bodies described by ALE–ANCF," *Nonlinear Dyn.*, vol. 93, no. 2, pp. 413–441, Jul. 2018, doi: 10.1007/s11071-018-4201-6.

[28] C. Q. Luo, J. L. Sun, H. Wen, and D. P. Jin, "Dynamics of a tethered satellite formation for space exploration modeled via ANCF," *Acta Astronautica*, vol. 177, pp. 882–890, Dec. 2020, doi: 10.1016/j.actaastro.2019.11.028.

[29] D. Garcída-Vallejo, J. Valverde, and J. Domínguez, "An internal damping model for the absolute nodal coordinate formulation," *Nonlinear Dyn.*, vol. 42, no. 4, pp. 347–369, Dec. 2005, doi: 10.1007/s11071-005-6445-1.

[30] G. M. Siouris, "Gravity modeling in aerospace applications," *Aerosp. Sci. Technol.*, vol. 13, no. 6, pp. 301–315, Sep. 2009, doi: 10.1016/j.ast.2009.05.005.

[31] H. D. Curtis, *Orbital Mechanics for Engineering Students*. Oxford, U.K.: Butterworth-Heineman, 2013.

[32] A. A. Shabana, "ANCF reference node for multibody system analysis," *Proc. Inst. Mech. Eng., K, J. Multi-Body Dyn.*, vol. 229, no. 1, pp. 109–112, Mar. 2015, doi: 10.1177/1464419314546342.

[33] M. Arnold and O. Brüls, "Convergence of the generalized-α scheme for constrained mechanical systems," *Multibody Syst. Dyn.*, vol. 18, no. 2, pp. 185–202, Aug. 2007, doi: 10.1007/s11044-007-9084-0.

[34] Z. Chu, J. Di, and J. Cui, "Hybrid tension control method for tethered satellite systems during large tumbling space debris removal," *Acta Astronautica*, vol. 152, pp. 611–623, Nov. 2018, doi: 10.1016/j.actaastro.2018.09.016.

[35] A. Steindl, W. Steiner, and H. Troger, "Optimal control of retrieval of a tethered subsatellite," in *IUTAM Symposium on Chaotic Dynamics and Control of Systems and Processes in Mechanics* (Solid Mechanics and its Applications), vol. 122, no. 3. Dordrecht, The Netherlands: Springer, 2005, pp. 441–450, doi: 10.1007/1-4020-3268-4_41.

[36] H. Pernicka, M. Dancer, A. Abrudan, and J. Harrington, "Simulation of the dynamics of a short tethered satellite system," in *Proc. AIAA/AAS Astrodynamics Spec. Conf. Exhibit*, Aug. 2004, vol. 3, no. 8, pp. 1429–1441, doi: 10.2514/6.2004-5311.

[37] P. Zheng, X. Cao, and S. Zhang, "J_2 perturbation effect on the deployment of tether-assisted deorbit system," in *Proc. 2nd Int. Symp. Syst. Control Aerosp. Astronaut.*, Dec. 2008, pp. 1–5.

ZHENGFENG BAI received the bachelor's, master's, and Ph.D. degrees in aeronautical and astronautical science and technology from the Harbin Institute of Technology, Harbin, China, in 2005, 2007, and 2011, respectively. He is currently an Associate Professor with the Department of Mechanical Engineering, Harbin Institute of Technology, Weihai. His research interests include multibody system dynamics, contact dynamics, structural dynamics and its applications in aerospace engineering, mechanical engineering, and so on.

XIN JIANG is currently pursuing the Ph.D. degree with the Department of Astronautic Engineering, Harbin Institute of Technology, Harbin, China. His research interests include multibody dynamics and structural dynamics.